Atmos. Chem. Phys. Discuss., 14, 11493–11539, 2014
www.atmos-chem-phys-discuss.net/14/11493/2014/
doi:10.5194/acpd-14-11493-2014

Atmospheric Chemistry and Physics Discussions
Open Access

Inverse modeling of CH_4 emissions for 2010–2011 using different satellite retrieval products from GOSAT and SCIAMACHY

M. Alexe[1], P. Bergamaschi[1], A. Segers[2], R. Detmers[3], A. Butz[9], O. Hasekamp[3], S. Guerlet[3], R. Parker[4], H. Boesch[4], C. Frankenberg[5], R. A. Scheepmaker[3], E. Dlugokencky[6], C. Sweeney[6,7], S. C. Wofsy[8], and E. A. Kort[10]

[1]European Commission, Joint Research Centre, Institute for Environment and Sustainability, Air and Climate Unit, Ispra, Italy
[2]Netherlands Organisation for Applied Scientific Research (TNO), Utrecht, the Netherlands
[3]Netherlands Institute for Space Research (SRON), Utrecht, the Netherlands
[4]Earth Observation Science Group, Space Research Centre, University of Leicester, Leicester, UK
[5]Jet Propulsion Laboratory, California Institute of Technology, Pasadena, California, USA
[6]Global Monitoring Division, NOAA Earth System Research Laboratory, Boulder, Colorado, USA
[7]CIRES, University of Colorado, Boulder, Colorado, USA

[8]School of Engineering and Applied Science and Department of Earth and Planetary Sciences, Harvard University, Cambridge, Massachusetts, USA
[9]Karlsruhe Institute of Technology (KIT), Karlsruhe, Germany
[10]Department of Atmospheric, Oceanic and Space Sciences, University of Michigan, Michigan, USA

Received: 13 March 2014 – Accepted: 13 April 2014 – Published: 8 May 2014

Correspondence to: M. Alexe (mihai.alexe@jrc.ec.europa.eu)

Published by Copernicus Publications on behalf of the European Geosciences Union.

Abstract

Beginning in 2009 new space-borne observations of dry-air column-averaged mole fractions of atmospheric methane (XCH_4) became available from the Thermal And Near infrared Sensor for carbon Observations–Fourier Transform Spectrometer (TANSO-FTS) instrument onboard the Greenhouse Gases Observing SATellite (GOSAT). Until April 2012 concurrent CH_4 measurements were provided by the SCanning Imaging Absorption spectroMeter for Atmospheric CartograpHY (SCIAMACHY) instrument onboard ENVISAT. The GOSAT and SCIAMACHY XCH_4 retrievals can be compared during their circa 32 month period of overlap. We estimate monthly average CH_4 emissions between January 2010 and December 2011, using the TM5-4DVAR inverse modeling system. Additionally, high-accuracy measurements from the National Oceanic and Atmospheric Administration Earth System Research Laboratory (NOAA ESRL) global air sampling network are used, providing strong constraints of the remote surface atmosphere. We discuss five inversion scenarios that make use of different GOSAT and SCIAMACHY XCH_4 retrieval products, including two sets of GOSAT proxy retrievals processed independently by the Netherlands Institute for Space Research (SRON)/Karlsruhe Institute of Technology (KIT), and the University of Leicester (UL), and the RemoTeC "Full-Physics" (FP) XCH_4 retrievals available from SRON/KIT. 2 year average emission maps show a good overall agreement among all GOSAT-based inversions, and compared to the SCIAMACHY-based inversion, with consistent flux adjustment patterns, particularly across Equatorial Africa and North America. The inversions are validated against independent shipboard and aircraft observations, and XCH_4 measurements available from the Total Carbon Column Observing Network (TCCON). All GOSAT and SCIAMACHY inversions show very similar validation performance.

ACPD
14, 11493–11539, 2014

1 Introduction

Atmospheric methane (CH_4) is the second-most important greenhouse gas (GHG) – after carbon dioxide – in terms of net radiative forcing. The CH_4 emission-based radiative forcing is estimated at $0.97\,W\,m^{-2}$ (Stocker et al., 2013), about twice the concentration-based estimate ($0.48\,W\,m^{-2}$). After a period of stabilization from 1999 to 2006 (Dlugokencky et al., 2003; Simpson et al., 2006), methane concentrations in the atmosphere have started to rise again (Dlugokencky et al., 2009; Rigby et al., 2008; Nisbet et al., 2014), and are currently estimated to be 160 % higher than pre-industrial (1750) values (WMO, 2013). Previous research has identified the main sources and sinks of atmospheric methane; however, there remain considerable uncertainties regarding their relative importance (e.g., Kirschke et al., 2013).

Since large-scale regional or global methane fluxes cannot be directly measured, attempts at estimating these quantities have traditionally relied on two complementary techniques: "bottom-up" emission inventories, and inverse modeling ("top-down"). Bayesian inverse modeling (Tarantola, 2004) of CH_4 emissions operates under a well-defined mathematical framework to combine a priori information on methane emissions, atmospheric observations, and an atmospheric chemistry and transport model (CTM), to yield a statistical best estimate of methane emissions and concentrations over the time period of interest. The quality of the estimates obtained through inverse modeling depends in large part on the quality of the observation data available for the spatial and temporal domains of interest, and the quality of the CTM.

Surface measurements of CH_4 concentrations are available from global networks such as the Earth System Research Laboratory of the National Oceanic and Atmospheric Administration (NOAA/ESRL) (Dlugokencky et al., 1994, 2009, 2013). However, surface observations provide only sparse global coverage, with the exception of certain regions, mainly Europe and North America, where regional monitoring stations, including tall towers and aircraft profiles, have been set up in recent years (Vermeulen et al., 2007). Surface measurements provide effective constraints on regional

ACPD
14, 11493–11539, 2014

emissions (Bergamaschi et al., 2010; Kort et al., 2008; Miller et al., 2013); however, they are not available in many important emission regions, such as the tropics. Inversions based on global background sites have provided a good picture of global and continental methane emissions, their trends, and inter-annual variability (Bergamaschi et al., 2013a; Houweling et al., 1999; Bousquet et al., 2006; Hein et al., 1997; Mikaloff Fletcher et al., 2004a, b). Smaller-scale regional patterns, however, remain in large part determined by the prior emission inventories.

Since the year 2003 satellite measurements of total-column methane mixing ratios have been available from the SCanning Imaging Absorption spectroMeter for Atmospheric CHartographY (SCIAMACHY) instrument onboard ENVISAT (Frankenberg et al., 2005, 2006, 2008, 2011; Buchwitz et al., 2005; Schneising et al., 2012). The SCIAMACHY data were the first space-borne XCH_4 retrievals sensitive to the atmospheric boundary layer. This consideration, along with an extension in data coverage to previously observation-poor areas, such as the tropics, led to the first global and regional inversions of methane concentrations and fluxes (Bergamaschi et al., 2007, 2009; Frankenberg et al., 2008; Meirink et al., 2008a). Due to the relatively long operational lifetime of SCIAMACHY (almost one decade), the XCH_4 retrievals from this instrument were useful for analysing the inter-annual methane variability (IAV) during this period (Bergamaschi et al., 2013a). However, the impact of the serious detector pixel degradation, which occurred at the end of 2005, remains difficult to evaluate, despite overall good consistency of the SCIAMACHY time series with surface observations (Frankenberg et al., 2011).

Since 2009, XCH_4 retrievals have also become available from the Greenhouse Gases Observing SATellite (GOSAT) TANSO-FTS instrument (Parker et al., 2011; Yoshida et al., 2011; Butz et al., 2011). Given the limited lifetime of satellite instruments (the communication link to ENVISAT was lost in April 2012, while the GOSAT mission plans extend only until 2014), inverse modeling comparison studies using different satellite products are of great importance. Such analyses facilitate the transition to another satellite measurement dataset when current retrievals become unavailable, a cru-

ACPD
14, 11493–11539, 2014

cial requirement when using satellite data to analyse IAV and trends. Within the European project MACC-II ("Monitoring Atmospheric Composition and Climate – Interim Implementation") pre-operational "delayed-mode" CH_4 flux inversions are performed, which are updated every six months (Bergamaschi et al., 2013b). Beginning in 2012 the assimilated satellite data set changed from SCIAMACHY IMAPv5.5 to GOSAT RemoTeC v2.0 (Bergamaschi et al., 2013b). Furthermore, alternative XCH_4 products from GOSAT and SCIAMACHY have been developed within the European Space Agency GHG Climate Change Initiative (ESA-GHG CCI) project (Buchwitz et al., 2013).

This study will present a detailed comparison of global CH_4 flux inversions constrained by different GOSAT and SCIAMACHY retrieval products and surface measurements, covering the two-year period between January 2010 and December 2011. The availability of multiple satellite retrieval products covering the same time interval allows for a detailed comparison of their consistency and added value in inverse modeling, which is the main objective of this paper. Three very recent inverse modeling studies (Fraser et al., 2013; Monteil et al., 2013; Cressot et al., 2014) have made use of SCIAMACHY and GOSAT measurements to estimate global CH_4 fluxes and concentrations. Our approach differs significantly from that of these studies. Herein we examine an extended time period, use a different inversion set-up, and employ several distinct (optimized) bias correction strategies for the SCIAMACHY and GOSAT measurements. Another novel element of this paper is the comparison of two different satellite proxy retrievals: the GOSAT RemoTeC dataset (Schepers et al., 2012) from SRON/KIT, and the OCPR GOSAT retrievals from the University of Leicester (Parker et al., 2011). We also assimilate the "Full-Physics" (FP) GOSAT retrievals from SRON/KIT, which do not require the use of modeled CO_2 fields. Furthermore, we invert the SCIAMACHY IMAPv5.5 retrievals as used in the MACC reanalysis (Bergamaschi et al., 2013a). In addition to the GOSAT and SCIAMACHY satellite retrievals, all inversions are constrained by high-accuracy CH_4 data from the NOAA/ESRL air sampling network. We also present a detailed validation of the inversion results against independent NOAA ship and aircraft profile samples, the aircraft transects from HIPPO – the

ACPD
14, 11493–11539, 2014

High-performance Instrumented Airborne Platform for Environmental Research (HIAPER) Pole-to-Pole observation campaigns from 2010 and 2011, and XCH_4 measurements from the Total Carbon Column Observation Network (TCCON) Fourier Transform Spectrometer (FTS) (Wunch et al., 2010). Finally, we discuss the impact of several bias correction approaches on the estimated total emissions.

This paper is organized as follows. Section 2 summarizes the main characteristics of the satellite and surface observations used in the inversion. The inverse modeling framework is described briefly in Sect. 3. In Sect. 4, we present and discuss the CH_4 emission estimates for the various inversion scenarios, and the validation of the model simulations against independent measurement data. Finally, the conclusions of the study are summarized in Sect. 5.

2 Observations

Table 1 gives an overview of the satellite data used in the inversions. The following sub-sections briefly discuss the characteristics of each set of satellite retrievals. For further details the reader is referred to, e.g., Parker et al. (2011); Butz et al. (2011); Frankenberg et al. (2011); Schepers et al. (2012).

2.1 The GOSAT retrievals

The Thermal And Near red infrared Sensor for carbon Observation (TANSO)–Fourier Transform Spectrometer (FTS), onboard the satellite GOSAT (launched by JAXA in January 2009), aims to provide measurements of atmospheric methane concentrations that have sufficient accuracy for use in global and regional CH_4 source and sink inversions. Column-averaged dry-air mole fractions are retrieved from a short-wave-infrared (SWIR) spectral analysis of sunlight backscattered by the Earth's surface and atmosphere.

ACPD
14, 11493–11539, 2014

The proxy retrieval algorithms rely on the small spectral distance between carbon dioxide and methane sunlight absorption bands (1.65 µm for CH_4 and 1.6 µm for CO_2), using the CO_2 column-average dry-air mole fraction (XCO_2) as proxy for the sampled air mass. This helps minimize systematic errors which may arise due to aerosol scattering and instrument-related effects.

The equation used to obtain the XCH_4 reads as follows:

$$XCH_4 = \frac{[CH_4]_{GOSAT}}{[CO_2]_{GOSAT} \times XCO_{2modeled}}. \quad (1)$$

The proxy retrieval algorithms considered herein use different XCO_2 model fields. The OCPR (OCO-Proxy) version 4 retrieval algorithm (Parker et al., 2011) from the University of Leicester (UL), developed under the ESA GHG-CCI initiative, derives the volume mixing ratios (VMRs) of carbon dioxide from the LMDZ model (Chevallier et al., 2010). The RemoTeC Proxy algorithm (version 1.9/2.0) (Schepers et al., 2012) uses modeled CO_2 total columns (XCO_{2CT}) obtained from CarbonTracker (Peters et al., 2007), with optimized carbon dioxide fields for 2010. For the years 2011 and 2012, the CO_2 fields are the same as in 2010, with an adjustment of 2 µmol mol^{-1} (ppm) for 2011, and 4 ppm for 2012, to account for the increase of atmospheric CO_2. Perturbations in the optical path will mostly cancel out when taking the ratio $\frac{[CH_4]_{GOSAT}}{[CO_2]_{GOSAT}}$ of the two measurements. However, Eq. (1) implies that errors in the modeled CO_2 columns propagate directly into the derived XCH_4. The quality of total column methane measurements depends thus on the accuracy of the modeled carbon dioxide fields.

The third GOSAT data set used in this study are the RemoTeC FP version 2.1 retrievals processed by SRON/KIT (Butz et al., 2011). The methodology can be summarized as follows. CH_4 and CO_2 columns are retrieved simultaneously with three effective aerosol parameters (amount, size, and height) from GOSAT-FTS measurements at the O_2 A-band around 0.76 microns (µm), the CH_4 and CO_2 absorption bands around 1.6 µm, and the strong CO_2 absorption band around 2.0 µm. Dividing the CH_4 column by the dry air column from the European Centre for Medium-Range Weather Forecast

ACPD
14, 11493–11539, 2014

(ECMWF) ERA-Interim data, yields the methane dry air mixing ratios (XCH_4). The full physics approach does not require a proxy CO_2 field; instead, the amount of sunlight scattering is estimated directly, together with the XCH_4, from the measured spectra. However, this method can only account for a fraction of the total scattering (Butz et al., 2011). A further trade-off is the lower tolerance to cloud cover (i.e., the method requires a stricter cloud filter). Possible biases in the satellite data are corrected using XCH_4 observations from the Total Carbon Column Observation Network, or TCCON (Wunch et al., 2010), as anchor points.

The filter settings for the GOSAT SRON FP retrievals follow the approach of Butz et al. (2011). We use only observations taken over land (no sun-glint ocean data) that have been screened for clouds. Scenario S1-GOSAT-SRON-FP also assimilates M-gain data (recorded over highly reflective land surfaces). There are considerable differences in the total accepted pixel counts for the full physics vs. the GOSAT proxy methods. Furthermore, GOSAT has a generally much sparser spatial sampling (due to the FTS integration time) compared to SCIAMACHY. Table 3 reports the total number of satellite data points that were used in each scenario (see also Fig. 4).

2.2 The SCIAMACHY measurements

The SCIAMACHY Iterative Maximum A Posteriori (IMAP) version 5.5 retrievals used in this study (Frankenberg et al., 2011) are calculated through the proxy approach outlined above. The variations in the CO_2 atmospheric columns are accounted for through the use of modeled CarbonTracker carbon dioxide fields (Frankenberg et al., 2011). Problems with the detector on the SCIAMACHY instrument occurred unexpectedly at the end of 2005, and led to a considerable degradation of the instrument performance in the 1.6 µm region relevant for CH_4 retrievals. The main feature of the IMAP v5.5 algorithm that set it apart from its predecessor, version 5.0 (Frankenberg et al., 2008), is the extension of the timeseries beyond 2005, using a coherent, uniform pixel mask for the entire retrieval period, so as to minimize the impact of pixel degradation (Frankenberg et al., 2011). The pixel deterioration remains visible in the IMAP v5.5 retrievals (higher

ACPD
14, 11493–11539, 2014

noise levels are noticeable starting with November 2005). Nonetheless, comparisons with measurements at NOAA surface sites indicate a relatively good consistency of the satellite data time series (Frankenberg et al., 2011). There remain some systematic differences between IMAP v5.5 and v5.0 retrievals (Frankenberg et al., 2011; Bergamaschi et al., 2013a). Following Bergamaschi et al. (2013a), we use a re-processed version of the IMAP v5.5 retrievals. This version includes CarbonTracker release 2010 CO_2 fields for the year 2009, while CO_2 fields for years 2010 through 2012 are based on non-optimized TM5 forward model runs using optimized CO_2 emissions from previous years (Bergamaschi et al., 2013a).

We assimilate only satellite data over land between 50° N and 50° S. We also discard all pixels whose average surface elevation is not within 250 m of the TM5 model surface height (Bergamaschi et al., 2009, 2013a). To avoid spurious outliers that may have a large impact on the inversion, we filter out any SCIAMACHY or GOSAT XCH_4 measurements of less than 1500 nmol mol^{-1} (henceforth abbreviated as ppb), or larger than 2500 ppb.

A SCIAMACHY pixel covers a ground area of 30 km (along track) times 60 km (across track), whereas TANSO-FTS has a ground pixel resolution of 10.5 km (at nadir). Single GOSAT and SCIAMACHY XCH_4 measurements are averaged on a regular (longitude × latitude) 1° × 1° grid over the individual 3 h assimilation time slots. The TM5 XCH_4 are then obtained by vertical integration of the 3-D modeled CH_4 fields interpolated to the same 1° × 1° grid, using the averaging kernels of the SCIAMACHY and GOSAT retrievals (Bergamaschi et al., 2009).

2.3 The NOAA surface observations

All inversions use high-quality CH_4 dry-air mole fraction measurements from a subset of 30 NOAA ESRL sites (Dlugokencky et al., 2013), globally distributed as shown in Fig. 1. Due to the coarse 6° × 4° resolution of the model, we include only marine and continental background sites. Other locations, e.g., located near the coast or strongly influenced by sub-grid local sources, are excluded from the assimilation. Moreover, the

ACPD
14, 11493–11539, 2014

list contains only sites with sufficient data coverage for 2010–2011. The NOAA surface measurements are calibrated against the NOAA2004 methane standard scale, or, equivalently, the World Meteorological Organization Global Atmosphere Watch (WMO GAW) CH_4 mole fraction scale (Dlugokencky et al., 2005).

2.4 Measurement data used for validation

2.4.1 NOAA observations

The simulated methane mixing ratios from all inversions are evaluated against independent observations which have not been assimilated. First, modeled CH_4 mixing ratios are compared against NOAA ship cruise data acquired in 2010 and 2011. These observations allow us to evaluate the simulated concentrations in the marine boundary layer, downwind of continental sources. Further important validation data sources are the NOAA aircraft-based vertical profiles (across North America and the Pacific Ocean, http://www.esrl.noaa.gov/gmd/ccgg/aircraft/index.html, and Fig. 1), to validate the modeled methane vertical gradients in the troposphere.

2.4.2 HIPPO aircraft campaigns

Simulated CH_4 fields are also validated against campaigns 3, 4 and 5 of the HIAPER Pole-to-Pole Observations (HIPPO) program (Wofsy, 2011). These three campaigns were run during March/April 2010 (HIPPO-3), June–July 2011 (HIPPO-4), and August–September 2011 (HIPPO-5), for the most part over the Pacific Ocean (see Fig. 1), but also partially above North America (between 87° N and 67° S). The HIPPO data consist of continuous profiles between ca. 150 m and 8500 m altitude. Several profiles extend up to 14 km altitude. For details on the measurement process, which makes use of a quantum cascade laser spectrometer (QCLS), the reader is directed to the paper of Kort et al. (2012). In addition, air samples collected using the NOAA Programmable Flask Package were taken during the HIPPO campaigns. Comparison of QCLS mea-

ACPD
14, 11493–11539, 2014

surements and NOAA flask samples taken within the same 10 s interval showed a small bias in the HIPPO data which has been accounted for in our validation (see Fig. 10 and the Supplement): 6 ppb for HIPPO-3, 4.5 ppb for HIPPO-4, and 5.2 ppb for HIPPO-5.

2.4.3 TCCON total-column XCH_4 measurements

TCCON measures dry-air column-averaged mole fractions of atmospheric methane at several sites across the globe (Table T2 in the Supplement) using Fourier Transform Spectrometers. The TCCON XCH_4 observations have an estimated accuracy of 7 ppb, and a precision of 0.2 % (Wunch et al., 2010). Only stations with sufficient data coverage during 2010–2011 are used in the validation. The modeled XCH_4 at the TCCON site locations were calculated using the TCCON a priori profiles and averaging kernels (Rodgers and Connor, 2003).

3 Modeling

3.1 Inverse modeling with TM5-4DVAR

We estimate the monthly averages of CH_4 surface fluxes between January 2010 and December 2011 using the TM5-4DVAR inverse modeling system (Meirink et al., 2008b) We also incorporate the further developments described in Bergamaschi et al. (2009, 2010). The statistical best fit of the model-generated 3-D methane fields and observations is achieved by minimization of the following cost functional:

$$\mathcal{J}(\boldsymbol{x}) = \frac{1}{2}(\boldsymbol{x}-\boldsymbol{x}_{\mathrm{B}})^{\mathrm{T}}\mathbf{B}^{-1}(\boldsymbol{x}-\boldsymbol{x}_{\mathrm{B}}) + \frac{1}{2}\sum_{i=1}^{n}(\mathcal{H}_i(\boldsymbol{x})-\boldsymbol{y}_i)^{\mathrm{T}}\mathbf{R}_i^{-1}(\mathcal{H}_i(\boldsymbol{x})-\boldsymbol{y}_i). \quad (2)$$

Here $\boldsymbol{x} = (x_{\mathrm{conc}}, x_{\mathrm{em}}, s)$ is the state vector, which comprises the initial CH_4 fields at the beginning of each inversion series x_{conc}, the monthly average emissions x_{em}, and the bias parameters s (Bergamaschi et al., 2009, 2013a). The observations are denoted

ACPD
14, 11493–11539, 2014

by $\mathbf{y}$, while $\mathcal{H}(\boldsymbol{x})$ is the corresponding model simulation. Finally, $\mathbf{B}$ and $\mathbf{R}_i$ are the parameter and observation error covariance matrices, where the index i indicates the observation window (set to 3 h). Positivity of a posteriori CH_4 emissions is enforced through the application of a "semi-exponential" probability density function (PDF) for the a priori emissions $(x_{\mathrm{em}})_{\mathrm{B}}$ (Bergamaschi et al., 2009, 2010). This particular choice of a priori PDF introduces a non-linearity in Eq. (2). The 4DVAR functional $\mathcal{J}$ in Eq. (2) is minimized using the algorithm M1QN3 (Gilbert and Lemaréchal, 1989). The adjoint model (Meirink et al., 2008b; Krol et al., 2008) allows for an efficient computation of the gradient of $\mathcal{J}$ during the minimization process.

TM5 is an off-line transport model (Krol et al., 2005) driven by the ERA-Interim reanalysis meteorological data (Dee et al., 2011) from ECMWF. We use the standard TM5 version (cycle 1), with a global horizontal resolution of 6° × 4° (longitude-latitude), and 25 hybrid pressure vertical layers.

3.2 Inversion settings

The prior emission inventories are identical to those used by Bergamaschi et al. (2013a). We independently optimize four groups of CH_4 emissions: wetlands, rice, biomass burning, and other remaining sources (Bergamaschi et al., 2010, 2013a). A priori uncertainties for each emission category are set to 100 % (per model grid cell and month), with the exception of the "remaining sources" whose uncertainty is set to 50 %. Wetland, rice, and biomass burning emissions are assumed to be uncorrelated in time, to allow the maximum flexibility when optimizing their seasonal variation. As in Bergamaschi et al. (2010), the temporal correlation of the remaining emissions – assumed to have little seasonal variation – is set to 9.5 months. A Gaussian function of the spatial distance between model grid cells is used to model the spatial emission error correlations, using a correlation length of 500 km, for all emission categories and all scenarios. Horizontal error correlations in the initial methane fields are modeled using a similar Gaussian distance of 500 km, while error correlations in the vertical direc-

ACPD
14, 11493–11539, 2014

tion are described by the National Meteorological Center (NMC) method (Parrish and Derber, 1992; Meirink et al., 2008a).

In all inversions the tropospheric methane sink is simulated using hydroxyl (OH) radical fields from a TM5 full chemistry run using the Carbon Bond Mechanism 4 optimized based on methyl chloroform measurements (Bergamaschi et al., 2009, 2010, 2013a). The lifetime of OH radicals is calculated at 10.1 years (total CH_4 vs. tropospheric OH). The Modular Earth Sub-model System version 1 (Jöckel et al., 2006) from the European Centre Hamburg general circulation model (ECHAM) version 5 is used to parameterize the stratospheric chemical destruction of methane by OH, Cl, and the oxygen isotope $O^1(D)$, using sink averages from 1999–2002.

The number of optimization iterations required to minimize the cost function (Eq. 2) increases with the length of the assimilation window. For this reason, we have split all our inversions into 18 month blocks (Fig. 2), with 6 month spin-down periods (Bergamaschi et al., 2013a). Consecutive blocks overlap by 6 months. The first block starts on 1 January 2009; the third 18 month inversion block ends on 1 July 2012. The inversion for 2009 is considered as spin-up, and not further analysed in this study. The results for the 6 month spin-down periods are also not used in the analysis. A priori 3-D CH_4 concentration fields for 1 January 2009, are taken from a methane inversion constrained only by surface measurements (scenario S1-NOAA of Bergamaschi et al., 2013a), with the exception of scenario S1-SCIA, which uses the optimized concentrations from inversion S1-SCIA of Bergamaschi et al. (2013a). Sixty iterations of the M1QN3 optimization algorithm are used for the cost function minimization in each inversion block for all inversions which include satellite data, and 40 iterations for S1-NOAA (which assimilates only the NOAA surface data).

Initial CH_4 3-D fields are optimized only for the first inversion block. The other two 18 month blocks start on 1 January from the optimized initial fields of the previous inversion block. This methodology guarantees a closed methane budget across the entire inversion period, i.e., total sources minus total sinks yield the variation in the global CH_4 burden. Additionally, the spin-down periods ensure that surface fluxes for

ACPD
14, 11493–11539, 2014

2010–2011 are constrained by all available observations for at least 6 months after emission.

The inversion scenarios considered in this study are summarized in Table 2. Scenario S1-NOAA is intended as a baseline for all the other inversions; it uses only NOAA/ESRL surface station data. Scenarios S1-GOSAT-SRON-PX, S1-GOSAT-SRON-FP, and S1-GOSAT-UL-PX assimilate both surface and GOSAT XCH_4 retrievals, whereas S1-SCIA uses SCIAMACHY retrievals and NOAA surface observations. The S1-satellite inversions make use of a second-order polynomial bias correction scheme that is a function of latitude and month (Bergamaschi et al., 2009, 2013a).

To assess the impact of the bias correction scheme on the posterior emission estimates, we have considered four additional scenarios: S2-GOSAT-SRON-FP, S3-GOSAT-SRON-FP, S2-GOSAT-UL-PX and S3-GOSAT-UL-PX. These differ from S1-GOSAT-SRON-FP and S1-GOSAT-UL-PX by their bias correction scheme. Inversions S3-GOSAT-SRON-FP and S3-GOSAT-UL-PX use a "smooth" bias correction (Bergamaschi et al., 2013a): one bias parameter per degree of latitude and month, 10 ppb prior uncertainty, and a prescribed 20° latitude Gaussian error correlation length. The bias correction coefficients used for S2-GOSAT-SRON-FP and S2-GOSAT-UL-PX are variable in time, but constant with latitude. The choice of bias correction scheme is not found to have a significant impact on the posterior regional emission estimates (shown in Table 4).

The aim of this study is to quantify the impact of the different satellite retrievals on the inverted methane fluxes and concentrations. Hence, all inversions use the same a priori emission inventories (as in Bergamaschi et al., 2013a), and identical OH fields. It is important to note that the high-accuracy surface observations act as constraints (or "anchor points") for the bias correction scheme.

ACPD
14, 11493–11539, 2014

4 Results and discussion

4.1 Assimilation statistics

The posterior statistics of S1-NOAA through S1-SCIA are summarized in Table 3. Figure 3 shows the frequency distributions of fit residuals (difference between model and observations). The data in Table 3 show that the bias is close to zero for both surface measurements and satellite XCH_4. Moreover, the model performance at the NOAA sites remains virtually identical when satellite data are assimilated: comparing the satellite-based inversions with S1-NOAA we note only a marginal increase in the bias of 0.1–0.2 ppb, and in the RMS difference of about 0.3–0.9 ppb (see also Fig. 3). The statistics of the three GOSAT inversions are almost identical in terms of posterior bias, standard deviation, and RMS difference between retrieved and assimilated XCH_4. While the large global bias in the SCIAMACHY XCH_4 retrievals is for the most part compensated by the bias correction mechanism (Fig. 4), the standard deviation of the posterior distribution of SCIAMACHY–TM5 fit residuals is much larger than that of the GOSAT inversions: $\sigma = 32$ ppb for S1-SCIA vs. an average standard deviation of 9–10 ppb for S1-GOSAT-SRON-PX through S1-GOSAT-UL-PX. The significantly lower standard deviations of the fit residuals obtained in all the GOSAT-based inversions (compared with SCIAMACHY) demonstrate the much higher precision of the GOSAT XCH_4 products. We note that the GOSAT inversions presented by Monteil et al. (2013) yielded a higher standard deviation (14.7–15.8 ppb). Since they used a previous retrieval version (RemoTeC Proxy v1.0 and Full-Physics v1.0 XCH_4), the lower standard deviation obtained in our study may reflect the further improvement of the GOSAT retrievals. Furthermore, the optimization of the bias correction probably plays some role: while Monteil et al. (2013) applied a constant correction to the GOSAT full physics retrievals before the inversion, based on the comparison with the TCCON data, they did not use any bias correction for the GOSAT proxy retrievals.

ACPD
14, 11493–11539, 2014

4.2 Modeled XCH_4

Figure 4 shows the column-averaged methane mixing ratios for 2010–2011 (2 year averages). The bias-corrected XCH_4 retrievals are plotted in the left maps, while the right-hand side maps show the assimilated XCH_4. Note the much denser data coverage of the SCIAMACHY XCH_4 retrievals (last row of Fig. 4) compared to that of the GOSAT products. For GOSAT, the more stringent selection criteria applied to the full-physics retrievals result in significantly lower pixel density than that achieved by the two proxy XCH_4 retrievals (see also Table 3).

The 4DVAR assimilation system is able to capture most major regional patterns of the observed XCH_4 fields, e.g., the pronounced XCH_4 enhancements over southeast Asia. Over Tropical South America, the agreement between retrieved and assimilated XCH_4 patterns is generally better for the three GOSAT-based inversions than for SCIAMACHY (e.g., over Columbia and Venezuela). Note, however, the lower data density of the GOSAT retrievals (especially of the GOSAT Full Physics retrievals) over those areas compared to SCIAMACHY. The different GOSAT products show overall very good consistency regarding the spatial XCH_4 patterns (in particular the two GOSAT proxy retrievals), and result in only small to moderate calculated bias corrections (maximum 10–20 ppb), indicating good consistency with the high-accuracy surface observations. In contrast, the SCIAMACHY XCH_4 require a significantly higher bias correction (varying with latitude by up to ca. 40 ppb). There are various indications that the SCIAMACHY IMAP v5.5 XCH_4 have a complex bias structure (e.g., the comparison with previous IMAP v5.0 XCH_4 retrievals examined by (Frankenberg et al., 2011)), which cannot be fully compensated by our polynomial bias correction. Furthermore, Houweling et al. (2013) showed recently that the bias of the SCIAMACHY IMAP v5.5 retrievals is strongly correlated with water vapour.

ACPD
14, 11493–11539, 2014

4.3 Inverted methane fluxes

Figure 6 shows the spatial distribution of emissions, averaged over the two years (2010–2011). The maps on the left side show the a priori (top) and a posteriori fluxes, while the middle panel shows the longitudinal average partitioning among the 4 source categories optimized in the inversions. The right-hand side maps display the differences between a posteriori and a priori emissions for our baseline inversion S1-NOAA, and for the satellite inversions S1-GOSAT-SRON-PX through S1-SCIA the difference between the a posteriori emissions of these inversions and S1-NOAA. While the satellite inversions yield significantly different spatial emission patterns compared to the NOAA-only inversion (due to the constraints of the satellite data over the continents), they show overall good qualitative agreement across all satellite inversions. This is visible in particular in the difference plots on the right side, showing similar regional emission increments relative to the NOAA-only inversion, especially over Tropical Africa and the United States. While the NOAA-only inversion results in a significant increase of the emission hot spot over the Congo Basin (which is a prominent feature in the applied wetland inventory, see Bergamaschi et al., 2007, 2009), all satellite inversions reduce the emissions from this hotspot significantly, and instead increase the emissions in eastern tropical Africa. Note that S1-GOSAT-SRON-FP calculates slightly lower emission rates for Equatorial Africa, likely due to the absence of observations available directly over that region (Fig. 4). For the US, the satellite inversions result in a redistribution of CH_4 emissions from the Northeastern USA to the middle south. The net increase in the emissions over the United States is consistent with recent estimates of Miller et al. (2013), and may be correlated to oil and gas industry activities in the region. While the coarse resolution of the model used in this study, and limitations of the inverse modeling system in differentiating between different source categories, do not allow to attribute these positive emission increments to specific sources, the remarkable qualitative agreement between the GOSAT and SCIAMACHY inversions regarding

ACPD
14, 11493–11539, 2014

the redistribution of CH_4 emissions over the US, warrants a more in-depth analysis of methane emissions over the North-American continent.

Methane fluxes aggregated over the TRANSCOM regions (Gurney et al., 2008) are shown in Fig. 7, and Table 4. All inversions show a small increase in the 2 year global total emissions over the prior, from 1.4 Tg CH_4 yr^{-1} for S1-GOSAT-SRON-PX to 5 Tg CH_4 yr^{-1} for the SCIAMACHY-based S1-SCIA. Emissions in the mid latitudes of the Northern Hemisphere are reduced in all scenarios (mainly across Europe and Temperate Eurasia, see Fig. 7b) although there are considerable differences between the flux adjustments calculated for each inversion, ranging from −17 Tg CH_4 yr^{-1} for the GOSAT full-physics S1-GOSAT-SRON-FP, to −37.5 Tg CH_4 yr^{-1} for S1-SCIA. The negative increments in the Northern Hemisphere are compensated by across-the-board increases in tropical emissions (between 30° N and 30° S) over the prior, from 16.7 Tg CH_4 yr^{-1} for S1-GOSAT-SRON-PX, to 48.4 Tg CH_4 yr^{-1} for S1-SCIA. The net increase in the Southern Hemisphere fluxes can be mainly attributed to increased emissions over Brazil and sub-Equatorial Africa. Part of the net increase in the SH could be due to some bias in the inter-hemispheric mixing of TM5, as recently diagnosed by SF_6 simulations (Patra et al., 2011; Monteil et al., 2013), and will be further investigated in subsequent studies.

Monteil et al. (2013) have reported that inversions using the GOSAT SRON proxy retrievals led to larger Asian emissions than those estimated using the SRON full-physics XCH_4 data set. We noticed a similar pattern in our inversions, particularly above tropical Asia where S1-GOSAT-SRON-FP flux estimates are circa 5.6 Tg CH_4 yr^{-1} lower than those of the GOSAT SRON proxy scenario S1-GOSAT-SRON-PX. Schepers et al. (2012) attribute this discrepancy in the emission estimates to a regional overestimation of CH_4 mixing ratios in the proxy retrieval algorithm, caused by deficiencies in the applied CO_2 fields. The two GOSAT proxy retrievals yield overall relatively similar emission patterns. There are, however, some differences in the exact magnitude of the regional-scale fluxes calculated by S1-GOSAT-SRON-PX and S1-GOSAT-UL-PX, e.g.,

ACPD
14, 11493–11539, 2014

a larger decrease in temperate Eurasian fluxes when the GOSAT OCPR retrievals are assimilated (see Fig. 6).

4.4 Model validation

All the inversion results are thoroughly validated against independent measurement data sets covering the atmospheric boundary layer (BL), the free troposphere (FT), as well as the upper troposphere and lower stratosphere (UTLS). Since the observations considered for validation have not been used in the assimilation, they provide an independent verification of the modeled XCH_4. Figure 8 gives an overview of the results for all inversions and validation data sets (for a total of slightly more than 80 900 observations). See Sect. 2.4 and Fig. 1 for details on each data set. The root mean square (RMS) differences shown in Fig. 8 have been averaged over all available measurements during 2010–2011. In general the optimized CH_4 mixing ratios have lower RMS differences than the prior concentrations. It is important to note that the a priori shown in Fig. 8 is already partly optimized, given that inversion blocks 2 and 3 (for 2010, and 2011, respectively) start from optimized initial fields (see the discussion in Sect. 3.2).

4.4.1 TCCON XCH_4 data

TCCON provides high-accuracy measurements of CH_4 concentrations at globally distributed locations using ground-based Fourier Transform Spectrometers (Wunch et al., 2010). We compare our modeled XCH_4 with the measurements reported by TCCON (GGG2012 data). Figure 9 shows the bias and RMS difference between the TM5 and TCCON XCH_4, averaged over the entire inversion period. Only stations with sufficient measurement data coverage for 2010–2011 are shown. The grey bars indicate the a priori bias and RMS (taken from S1-NOAA). There is a noticeable improvement in the bias over the prior at the northernmost TCCON stations in Fig. 9. At other regional stations the improvement is modest, and at some stations, e.g., at Four-Corners (FCO), the XCH_4 bias slightly deteriorates after the assimilation. We note, however,

ACPD
14, 11493–11539, 2014

that methane concentrations at Four-Corners may be influenced by regional sources, such as nearby power stations.

We note a systematic trend in the bias from north to south (except for FCO). The positive bias at high northern latitudes could be partly due to overestimated CH_4 mixing ratios in the stratosphere (see the comparison of Bergamaschi et al. (2009) with balloon measurements, and comparisons with HIPPO data in Sect. 4.4.2 and Fig. 10). However, there is also some uncertainty in the TCCON FTS data, since the stratospheric contribution is not directly calibrated and validated (Wunch et al., 2010; Geibel et al., 2012). In future studies, the AirCore CH_4 measurements from NOAA/ESRL (Karion et al., 2010) may also serve as an independent benchmark of both model and TCCON XCH_4 in the stratosphere.

4.4.2 HIPPO aircraft campaigns

Figure 10 shows the bias corrected HIPPO data for all three campaigns (leftmost panels), and modeled mixing ratios for scenario S1-GOSAT-SRON-PX. There is overall a good agreement between the model simulations and the HIPPO observations (similar results for scenarios S1-GOSAT-SRON-FP through S1-SCIA are reported in the Supplement).

The rightmost panels in Fig. 10 show the average bias as a function of altitude and latitude band: extra-tropical NH (reed points), tropics (light green), and extra-tropical SH regions (blue). Agreement between model simulations and the HIPPO measurements in the free troposphere is generally very good for all inversions. However, the bias increases significantly above 300 hPa for all three HIPPO campaigns, particularly in the extra-tropical regions. A similar bias pattern has been reported by Bergamaschi et al. (2013a, Fig. 10). This abrupt deterioration of model performance in the stratosphere is likely caused by deficiencies of the parameterization of the stratospheric sink at high latitudes, and the inability of the coarse-resolution TM5 model to resolve the small-scale dynamics of the stratospheric–tropospheric exchange.

ACPD
14, 11493–11539, 2014

5 Conclusions

This study compares several inversions of global CH_4 emissions for 2010–2011, using four different satellite XCH_4 products: the SCIAMACHY IMAPv5.5 retrievals (Frankenberg et al., 2011), the SRON/KIT GOSAT RemoTeC Proxy v1.9/v2.0 and Full-Physics v2.1 (Butz et al., 2011; Schepers et al., 2012) retrievals, and the GOSAT OCPR v4.0 product from the University of Leicester (Parker et al., 2011). All inversions considered herein are further constrained by high-accuracy methane measurement data from the NOAA/ESRL global station network (Dlugokencky et al., 2013). The modeled 3-D CH_4 fields have been validated against multiple sets of independent observations that were not assimilated.

The inversion results demonstrate clear improvements in the quality of the GOSAT XCH_4 retrievals over SCIAMACHY, both in terms of precision, and accuracy. The standard deviations of the model to observation fit residuals of the GOSAT-based inversions (9–10 ppb) are significantly lower than the value calculated for the SCIAMACHY scenario (~ 32 ppb). Furthermore, the monthly bias corrections applied to the GOSAT retrievals (Fig. 4) are only a fraction of those estimated for the SCIAMACHY measurements. All the satellite inversions yield qualitatively consistent regional emission patterns, particularly over Tropical Africa and the United States. The inversions highlight areas of increased methane emissions over the southwestern USA, a result consistent with the recent estimates of Miller et al. (2013). While there remain some quantitative differences between the emission increments retrieved by each scenario, the 2 year average regional fluxes for the TRANSCOM regions with the largest contributions, generally agree to within 10 Tg CH_4 yr^{-1} after the assimilation. For the GOSAT UL Proxy and SRON Full-Physics scenarios, the retrieved regional emission estimates show little sensitivity to the particular choice of optimized bias correction scheme (Table 4).

The satellite inversions show similar validation performance. The posterior CH_4 mixing ratios have, in general, a lower RMS difference to the observations than the prior concentrations. However, validation against the HIPPO profiles demonstrates that

ACPD
14, 11493–11539, 2014

a significant bias remains present in the UTLS at higher latitudes, indicating possible deficiencies of the parameterization of the stratospheric sink, or potentially also transport within the stratosphere. Furthermore, increased horizontal and vertical model resolutions may improve the representation of stratospheric–tropospheric exchange, leading to a better agreement with observations in the upper atmosphere. The observed deficiencies of TM5 in the UTLS and stratosphere at high latitudes may partly explain the noticeable north-south trend in the bias between TM5 and TCCON XCH_4 (Fig. 9).

Supplementary material related to this article is available online at http://www.atmos-chem-phys-discuss.net/14/11493/2014/ acpd-14-11493-2014-supplement.pdf.

Acknowledgements. The authors thank the TCCON PIs for making their measurement data available. The TCCON XCH_4 data (GGG2012) were obtained from the TCCON Data Archive, operated by the California Institute of Technology, and hosted at the website http://tccon.ipac.caltech.edu/. US funding for TCCON comes from NASA's Carbon Cycle Program, grant number NNX11AG01G, the Orbiting Carbon Observatory Program, and the DOE/ARM Program. The European TCCON groups involved in this study acknowledge financial support by the EU infrastructure project InGOS. The University of Bremen acknowledges financial support of the Bialystok and Orleans TCCON sites from the Senate of Bremen and EU projects IMECC, GEOmon and InGOS, as well as maintenance and logistical work provided by AeroMeteo Service (Bialystok) and the RAMCES team at LSCE (Gif-sur-Yvette, France), and additional operational funding from the National Institute for Environmental Studies (NIES, Japan). The authors acknowledge Nicholas Deutscher for his kind assistance with the TCCON data processing. This work has been supported by the European Commission Seventh Framework Programme (FP7/2007–2013) projects MACC under grant agreement 218793 and MACC-II under grant agreement 283576. The ECMWF meteorological data has been preprocessed by Philippe Le Sager into the TM5 input format. We thank Greet Janssens-Maenhout for providing the EDGARv4.2 emission inventory, and Christoph Brühl for providing the stratospheric CH_4 sinks from the ECHAM5/MESSy1 model. ECMWF has kindly provided the necessary computing resources, under the special project "Global and Regional Inverse Modeling of Atmospheric CH_4

ACPD
14, 11493–11539, 2014

and N_2O" (2012–2014). H. Boesch and R. Parker acknowledge funding by the NERC National Centre for Earth Observation and the ESA Climate Change Initiative. André Butz acknowledges support by the Emmy-Noether programme of the Deutsche Forschungsgemeinschaft (DFG) through grant number BU2599/1-1 (RemoteC).

References

Bergamaschi, P., Frankenberg, C., Meirink, J. F., Krol, M., Dentener, F., Wagner, T., Platt, U., Kaplan, J. O., Körner, S., Heimann, M., Dlugokencky, E. J., and Goede, A.: Satellite chartography of atmospheric methane from SCIAMACHY on board ENVISAT: 2. Evaluation based on inverse model simulations, J. Geophys. Res.-Atmos., 112, D02304, doi:10.1029/2006JD007268, 2007. 11497, 11510

Bergamaschi, P., Frankenberg, C., Meirink, J. F., Krol, M., Villani, M. G., Houweling, S., Dentener, F., Dlugokencky, E. J., Miller, J. B., Gatti, L. V., Engel, A., and Levin, I.: Inverse modeling of global and regional CH_4 emissions using SCIAMACHY satellite retrievals, J. Geophys. Res.-Atmos., 114, D22301, doi:10.1029/2009JD012287, 2009. 11497, 11502, 11504, 11505, 11506, 11507, 11510, 11513

Bergamaschi, P., Krol, M., Meirink, J. F., Dentener, F., Segers, A., van Aardenne, J., Monni, S., Vermeulen, A. T., Schmidt, M., Ramonet, M., Yver, C., Meinhardt, F., Nisbet, E. G., Fisher, R. E., O'Doherty, S., and Dlugokencky, E. J.: Inverse modeling of European CH_4 emissions 2001–2006, J. Geophys. Res.-Atmos., 115, D22309, doi:10.1029/2010JD014180, 2010. 11497, 11504, 11505, 11506

Bergamaschi, P., Houweling, S., Segers, A., Krol, M., Frankenberg, C., Scheepmaker, R. A., Dlugokencky, E., Wofsy, S. C., Kort, E. A., Sweeney, C., Schuck, T., Brenninkmeijer, C., Chen, H., Beck, V., and Gerbig, C.: Atmospheric CH_4 in the first decade of the 21st century: inverse modeling analysis using SCIAMACHY satellite retrievals and NOAA surface measurements, J. Geophys. Res.-Atmos., 118, 7350–7369, doi:10.1002/jgrd.50480, 2013a. 11497, 11498, 11502, 11504, 11505, 11506, 11507, 11513, 11528

Bergamaschi, P., Segers, A., Scheepmaker, R., Frankenberg, C., Hasekamp, O., Dlugokencky, E., Sweeney, C., Ramonet, M., Tarniewicz, J., Kort, E., and Wofsy, S.: Report on the quality of the inverted CH_4 fluxes, MACC-II Deliverable D_43.3, Tech. rep., available

at: https://www.gmes-atmosphere.eu/documents/maccii/deliverables/ghg/, Joint Research Center, European Commission, 2013b. 11498

Bousquet, P., Ciais, P., Miller, J. B., Dlugokencky, E. J., Hauglustaine, D. A., Prigent, C., Van der Werf, G. R., Peylin, P., Brunke, E.-G., Carouge, C., Langenfelds, R. L., Lathiere, J., Papa, F., Ramonet, M., Schmidt, M., Steele, L. P., Tyler, S. C., and White, J.: Contribution of anthropogenic and natural sources to atmospheric methane variability, Nature, 443, 439–443, doi:10.1038/nature05132, 2006. 11497

Buchwitz, M., de Beek, R., Burrows, J. P., Bovensmann, H., Warneke, T., Notholt, J., Meirink, J. F., Goede, A. P. H., Bergamaschi, P., Körner, S., Heimann, M., and Schulz, A.: Atmospheric methane and carbon dioxide from SCIAMACHY satellite data: initial comparison with chemistry and transport models, Atmos. Chem. Phys., 5, 941–962, doi:10.5194/acp-5-941-2005, 2005. 11497

Buchwitz, M., Reuter, M., Schneising, O., Boesch, H., Guerlet, S., Dils, B., Aben, I., Armante, R., Bergamaschi, P., Blumenstock, T., Bovensmann, H., Brunner, D., Buchmann, B., Burrows, J., Butz, A., Chédin, A., Chevallier, F., Crevoisier, C., Deutscher, N., Frankenberg, C., Hase, F., Hasekamp, O., Heymann, J., Kaminski, T., Laeng, A., Lichtenberg, G., Mazière, M. D., Noël, S., Notholt, J., Orphal, J., Popp, C., Parker, R., Scholze, M., Sussmann, R., Stiller, G., Warneke, T., Zehner, C., Bril, A., Crisp, D., Griffith, D., Kuze, A., O'Dell, C., Oshchepkov, S., Sherlock, V., Suto, H., Wennberg, P., Wunch, D., Yokota, T., and Yoshida, Y.: The Greenhouse Gas Climate Change Initiative (GHG-CCI): comparison and quality assessment of near-surface-sensitive satellite-derived CO_2 and CH_4 global data sets, Remote Sens. Environ., in press, doi:10.1016/j.rse.2013.04.024, 2013. 11498

Butz, A., Guerlet, S., Hasekamp, O., Schepers, D., Galli, A., Aben, I., Frankenberg, C., Hartmann, J.-M., Tran, H., Kuze, A., Keppel-Aleks, G., Toon, G., Wunch, D., Wennberg, P., Deutscher, N., Griffith, D., Macatangay, R., Messerschmidt, J., Notholt, J., and Warneke, T.: Toward accurate CO_2 and CH_4 observations from GOSAT, Geophys. Res. Lett., 38, L14812, doi:10.1029/2011GL047888, 2011. 11497, 11499, 11500, 11501, 11514

Chevallier, F., Ciais, P., Conway, T. J., Aalto, T., Anderson, B. E., Bousquet, P., Brunke, E. G., Ciattaglia, L., Esaki, Y., Fröhlich, M., Gomez, A., Gomez-Pelaez, A. J., Haszpra, L., Krummel, P. B., Langenfelds, R. L., Leuenberger, M., Machida, T., Maignan, F., Matsueda, H., Morguí, J. A., Mukai, H., Nakazawa, T., Peylin, P., Ramonet, M., Rivier, L., Sawa, Y., Schmidt, M., Steele, L. P., Vay, S. A., Vermeulen, A. T., Wofsy, S., and Worthy, D.: CO_2 surface fluxes at grid point scale estimated from a global 21 year reanalysis of atmospheric

measurements, J. Geophys. Res.-Atmos., 115, D21307, doi:10.1029/2010JD013887, 2010. 11500

Cressot, C., Chevallier, F., Bousquet, P., Crevoisier, C., Dlugokencky, E. J., Fortems-Cheiney, A., Frankenberg, C., Parker, R., Pison, I., Scheepmaker, R. A., Montzka, S. A., Krummel, P. B., Steele, L. P., and Langenfelds, R. L.: On the consistency between global and regional methane emissions inferred from SCIAMACHY, TANSO-FTS, IASI and surface measurements, Atmos. Chem. Phys., 14, 577–592, doi:10.5194/acp-14-577-2014, 2014. 11498

Dee, D. P., Uppala, S. M., Simmons, A. J., Berrisford, P., Poli, P., Kobayashi, S., Andrae, U., Balmaseda, M. A., Balsamo, G., Bauer, P., Bechtold, P., Beljaars, A. C. M., van de Berg, L., Bidlot, J., Bormann, N., Delsol, C., Dragani, R., Fuentes, M., Geer, A. J., Haimberger, L., Healy, S. B., Hersbach, H., Holm, E. V., Isaksen, L., Kållberg, P., Köhler, M., Matricardi, M., McNally, A. P., Monge-Sanz, B. M., Morcrette, J.-J., Park, B.-K., Peubey, C., de Rosnay, P., Tavolato, C., Thépaut, J.-N., and Vitart, F.: The ERA-Interim reanalysis: configuration and performance of the data assimilation system, Q. J. Roy. Meteor. Soc., 137, 553–597, doi:10.1002/qj.828, 2011. 11505

Dlugokencky, E. J., Steele, L. P., Lang, P. M., and Masarie, K. A.: The growth rate and distribution of atmospheric methane, J. Geophys. Res.-Atmos., 99, 17021–17043, doi:10.1029/94JD01245, 1994. 11496

Dlugokencky, E. J., Houweling, S., Bruhwiler, L., Masarie, K. A., Lang, P. M., Miller, J. B., and Tans, P. P.: Atmospheric methane levels off: Temporary pause or a new steady-state?, Geophys. Res. Lett., 30, 1992, doi:10.1029/2003GL018126, 2003. 11496

Dlugokencky, E. J., Myers, R. C., Lang, P. M., Masarie, K. A., Crotwell, A. M., Thoning, K. W., Hall, B. D., Elkins, J. W., and Steele, L. P.: Conversion of NOAA atmospheric dry-air CH_4 mole fractions to a gravimetrically prepared standard scale, J. Geophys. Res.-Atmos., 110, D18306, doi:10.1029/2005JD006035, 2005. 11503

Dlugokencky, E. J., Bruhwiler, L., White, J. W. C., Emmons, L. K., Novelli, P. C., Montzka, S. A., Masarie, K. A., Lang, P. M., Crotwell, A. M., Miller, J. B., and Gatti, L. V.: Observational constraints on recent increases in the atmospheric CH_4 burden, Geophys. Res. Lett., 36, L18803, doi:10.1029/2009GL039780, 2009. 11496

Dlugokencky, E., Lang, P. M., Crotwell, A. M., Masarie, K. A., and Crotwell, M. J.: Atmospheric methane dry-air mole fractions from the NOAA ESRL carbon cycle cooperative global air sampling network: 1988–2012, Version: 2013-06-18, available at: ftp://aftp.cmdl.noaa.gov/

data/trace_gases/ch4/flask/surface/ (last access: 18 November 2013), 2013. 11496, 11502, 11514

Frankenberg, C., Meirink, J. F., van Weele, M., Platt, U., and Wagner, T.: Assessing methane emissions from global space-borne observations, Science, 308, 1010–1014, doi:10.1126/science.1106644, 2005. 11497

Frankenberg, C., Meirink, J. F., Bergamaschi, P., Goede, A. P. H., Heimann, M., Körner, S., Platt, U., van Weele, M., and Wagner, T.: Satellite chartography of atmospheric methane from SCIAMACHY on board ENVISAT: analysis of the years 2003 and 2004, J. Geophys. Res.-Atmos., 111, D02304, doi:10.1029/2005JD006235, 2006. 11497

Frankenberg, C., Bergamaschi, P., Butz, A., Houweling, S., Meirink, J. F., Notholt, J., Petersen, A. K., Schrijver, H., Warneke, T., and Aben, I.: Tropical methane emissions: a revised view from SCIAMACHY onboard ENVISAT, Geophys. Res. Lett., 35, L15811, doi:10.1029/2008GL034300, 2008. 11497, 11501

Frankenberg, C., Aben, I., Bergamaschi, P., Dlugokencky, E. J., van Hees, R., Houweling, S., van der Meer, P., Snel, R., and Tol, P.: Global column-averaged methane mixing ratios from 2003 to 2009 as derived from SCIAMACHY: trends and variability, J. Geophys. Res.-Atmos., 116, D04302, doi:10.1029/2010JD014849, 2011. 11497, 11499, 11501, 11502, 11509, 11514

Fraser, A., Palmer, P. I., Feng, L., Boesch, H., Cogan, A., Parker, R., Dlugokencky, E. J., Fraser, P. J., Krummel, P. B., Langenfelds, R. L., O'Doherty, S., Prinn, R. G., Steele, L. P., van der Schoot, M., and Weiss, R. F.: Estimating regional methane surface fluxes: the relative importance of surface and GOSAT mole fraction measurements, Atmos. Chem. Phys., 13, 5697–5713, doi:10.5194/acp-13-5697-2013, 2013. 11498

Geibel, M. C., Messerschmidt, J., Gerbig, C., Blumenstock, T., Chen, H., Hase, F., Kolle, O., Lavrič, J. V., Notholt, J., Palm, M., Rettinger, M., Schmidt, M., Sussmann, R., Warneke, T., and Feist, D. G.: Calibration of column-averaged CH_4 over European TCCON FTS sites with airborne in-situ measurements, Atmos. Chem. Phys., 12, 8763–8775, doi:10.5194/acp-12-8763-2012, 2012. 11513

Gilbert, J. C. and Lemaréchal, C.: Some numerical experiments with variable-storage quasi-Newton algorithms, Math. Program., 45, 407–435, doi:10.1007/BF01589113, 1989. 11505

Gurney, K. R., Baker, D., Rayner, P., and Denning, S.: Interannual variations in continental-scale net carbon exchange and sensitivity to observing networks estimated from atmo-

spheric CO_2 inversions for the period 1980 to 2005, Global Biogeochem. Cy., 22, GB3025, doi:10.1029/2007GB003082, 2008. 11511

Hein, R., Crutzen, P. J., and Heimann, M.: An inverse modeling approach to investigate the global atmospheric methane cycle, Global Biogeochem. Cy., 11, 43–76, doi:10.1029/96GB03043, 1997. 11497

Houweling, S., Kaminski, T., Dentener, F., Lelieveld, J., and Heimann, M.: Inverse modeling of methane sources and sinks using the adjoint of a global transport model, J. Geophys. Res.-Atmos., 104, 26137–26160, doi:10.1029/1999JD900428, 1999. 11497

Houweling, S., Krol, M., Bergamaschi, P., Frankenberg, C., Dlugokencky, E. J., Morino, I., Notholt, J., Sherlock, V., Wunch, D., Beck, V., Gerbig, C., Chen, H., Kort, E. A., Röckmann, T., and Aben, I.: A multi-year methane inversion using SCIAMACHY, accounting for systematic errors using TCCON measurements, Atmos. Chem. Phys. Discuss., 13, 28117–28171, doi:10.5194/acpd-13-28117-2013, 2013. 11509

Jöckel, P., Tost, H., Pozzer, A., Brühl, C., Buchholz, J., Ganzeveld, L., Hoor, P., Kerkweg, A., Lawrence, M. G., Sander, R., Steil, B., Stiller, G., Tanarhte, M., Taraborrelli, D., van Aardenne, J., and Lelieveld, J.: The atmospheric chemistry general circulation model ECHAM5/MESSy1: consistent simulation of ozone from the surface to the mesosphere, Atmos. Chem. Phys., 6, 5067–5104, doi:10.5194/acp-6-5067-2006, 2006. 11506

Karion, A., Sweeney, C., Tans, P., and Newberger, T.: AirCore: an innovative atmospheric sampling system, J. Atmos. Ocean. Tech., 27, 1839–1853, doi:10.1175/2010JTECHA1448.1, 2010. 11513

Kirschke, S., Bousquet, P., Ciais, P., Saunois, M., Canadell, J. G., Dlugokencky, E. J., Bergamaschi, P., Bergmann, D., Blake, D. R., Bruhwiler, L., Cameron-Smith, P., Castaldi, S., Chevallier, F., Feng, L., Fraser, A., Heimann, M., Hodson, E. L., Houweling, S., Josse, B., Fraser, P. J., Krummel, P. B., Lamarque, J. F., Langenfelds, R. L., Le Quere, C., Naik, V., O'Doherty, S., Palmer, P. I., Pison, I., Plummer, D., Poulter, B., Prinn, R. G., Rigby, M., Ringeval, B., Santini, M., Schmidt, M., Shindell, D. T., Simpson, I., Spahni, R., Steele, L. P., Strode, S. A., Sudo, K., Szopa, S., van der Werf, G. R., Voulgarakis, A., van Weele, M., Weiss, R. F., Williams, J. E., and Zeng, G.: Three decades of global methane sources and sinks, Nat. Geosci., 6, 813–823, doi:10.1038/ngeo1955, 2013. 11496

Kort, E. A., Eluszkiewicz, J., Stephens, B. B., Miller, J. B., Gerbig, C., Nehrkorn, T., Daube, B. C., Kaplan, J. O., Houweling, S., and Wofsy, S. C.: Emissions of CH_4 and N_2O over the United States and Canada based on a receptor-oriented modeling framework and COBRA-NA

atmospheric observations, Geophys. Res. Lett., 35, L18808, doi:10.1029/2008GL034031, 2008. 11497

Kort, E. A., Wofsy, S. C., Daube, B. C., Diao, M., Elkins, J. W., Gao, R. S., Hintsa, E. J., Hurst, D. F., Jimenez, R., and Moore, F. L.: Atmospheric observations of Arctic Ocean methane emissions up to 82° north, Nat. Geosci., 5, 318–321, doi:10.1038/ngeo1452, 2012. 11503

Krol, M., Houweling, S., Bregman, B., van den Broek, M., Segers, A., van Velthoven, P., Peters, W., Dentener, F., and Bergamaschi, P.: The two-way nested global chemistry-transport zoom model TM5: algorithm and applications, Atmos. Chem. Phys., 5, 417–432, doi:10.5194/acp-5-417-2005, 2005. 11505

Krol, M. C., Meirink, J. F., Bergamaschi, P., Mak, J. E., Lowe, D., Jöckel, P., Houweling, S., and Röckmann, T.: What can ^{14}CO measurements tell us about OH?, Atmos. Chem. Phys., 8, 5033–5044, doi:10.5194/acp-8-5033-2008, 2008. 11505

Meirink, J. F., Bergamaschi, P., Frankenberg, C., d'Amelio, M. T. S., Dlugokencky, E. J., Gatti, L. V., Houweling, S., Miller, J. B., Röckmann, T., Villani, M. G., and Krol, M. C.: Four-dimensional variational data assimilation for inverse modeling of atmospheric methane emissions: analysis of SCIAMACHY observations, J. Geophys. Res.-Atmos., 113, D17301, doi:10.1029/2007JD009740, 2008. 11497, 11506

Meirink, J. F., Bergamaschi, P., and Krol, M. C.: Four-dimensional variational data assimilation for inverse modelling of atmospheric methane emissions: method and comparison with synthesis inversion, Atmos. Chem. Phys., 8, 6341–6353, doi:10.5194/acp-8-6341-2008, 2008b. 11504, 11505

Mikaloff Fletcher, S. E., Tans, P. P., Bruhwiler, L. M., Miller, J. B., and Heimann, M.: CH_4 sources estimated from atmospheric observations of CH_4 and its 13C/12C isotopic ratios: 1. Inverse modeling of source processes, Global Biogeochem. Cy., 18, GB4004, doi:10.1029/2004GB002223, 2004a. 11497

Mikaloff Fletcher, S. E., Tans, P. P., Bruhwiler, L. M., Miller, J. B., and Heimann, M.: CH_4 sources estimated from atmospheric observations of CH_4 and its 13C/12C isotopic ratios: 2. Inverse modeling of CH_4 fluxes from geographical regions, Global Biogeochem. Cy., 18, GB4005, doi:10.1029/2004GB002224, 2004b. 11497

Miller, S. M., Wofsy, S. C., Michalak, A. M., Kort, E. A., Andrews, A. E., Biraud, S. C., Dlugokencky, E. J., Eluszkiewicz, J., Fischer, M. L., Janssens-Maenhout, G., Miller, B. R., Miller, J. B., Montzka, S. A., Nehrkorn, T., and Sweeney, C.: Anthropogenic emis-

sions of methane in the United States, P. Natl. Acad. Sci. USA, 110, 20018–20022, doi:10.1073/pnas.1314392110, 2013. 11497, 11510, 11514

Monteil, G., Houweling, S., Butz, A., Guerlet, S., Schepers, D., Hasekamp, O., Frankenberg, C., Scheepmaker, R., Aben, I., and Röckmann, T.: Comparison of CH_4 inversions based on 15 months of GOSAT and SCIAMACHY observations, J. Geophys. Res.-Atmos., 118, 11807–11823, doi:10.1002/2013JD019760, 2013. 11498, 11508, 11511

Nisbet, E. G., Dlugokencky, E. J., and Bousquet, P.: Methane on the rise-again, Science, 343, 493–495, doi:10.1126/science.1247828, 2014. 11496

Parker, R., Boesch, H., Cogan, A., Fraser, A., Feng, L., Palmer, P. I., Messerschmidt, J., Deutscher, N., Griffith, D. W. T., Notholt, J., Wennberg, P. O., and Wunch, D.: Methane observations from the Greenhouse Gases Observing SATellite: comparison to ground-based TCCON data and model calculations, Geophys. Res. Lett., 38, L15807, doi:10.1029/2011GL047871, 2011. 11497, 11498, 11499, 11500, 11514

Parrish, D. F. and Derber, J. C.: The National Meteorological Center's spectral statistical-interpolation analysis system, Mon. Weather Rev., 120, 1747–1763, doi:10.1175/1520-0493(1992)120<1747:TNMCSS>2.0.CO;2, 1992. 11506

Patra, P. K., Houweling, S., Krol, M., Bousquet, P., Belikov, D., Bergmann, D., Bian, H., Cameron-Smith, P., Chipperfield, M. P., Corbin, K., Fortems-Cheiney, A., Fraser, A., Gloor, E., Hess, P., Ito, A., Kawa, S. R., Law, R. M., Loh, Z., Maksyutov, S., Meng, L., Palmer, P. I., Prinn, R. G., Rigby, M., Saito, R., and Wilson, C.: TransCom model simulations of CH_4 and related species: linking transport, surface flux and chemical loss with CH_4 variability in the troposphere and lower stratosphere, Atmos. Chem. Phys., 11, 12813–12837, doi:10.5194/acp-11-12813-2011, 2011. 11511

Peters, W., Jacobson, A. R., Sweeney, C., Andrews, A. E., Conway, T. J., Masarie, K., Miller, J. B., Bruhwiler, L. M. P., Pétron, G., Hirsch, A. I., Worthy, D. E. J., van der Werf, G. R., Randerson, J. T., Wennberg, P. O., Krol, M. C., and Tans, P. P.: An atmospheric perspective on North American carbon dioxide exchange: CarbonTracker, P. Natl. Acad. Sci. USA, 104, 18925–18930, doi:10.1073/pnas.0708986104, 2007. 11500

Rigby, M., Prinn, R. G., Fraser, P. J., Simmonds, P. G., Langenfelds, R. L., Huang, J., Cunnold, D. M., Steele, L. P., Krummel, P. B., Weiss, R. F., O'Doherty, S., Salameh, P. K., Wang, H. J., Harth, C. M., Mühle, J., and Porter, L. W.: Renewed growth of atmospheric methane, Geophys. Res. Lett., 35, L22805, doi:10.1029/2008GL036037, 2008. 11496

Rodgers, C. D. and Connor, B. J.: Intercomparison of remote sounding instruments, J. Geophys. Res.-Atmos., 108, 4116, doi:10.1029/2002JD002299, 2003. 11504

Schepers, D., Guerlet, S., Butz, A., Landgraf, J., Frankenberg, C., Hasekamp, O., Blavier, J.-F., Deutscher, N. M., Griffith, D. W. T., Hase, F., Kyro, E., Morino, I., Sherlock, V., Sussmann, R., and Aben, I.: Methane retrievals from Greenhouse Gases Observing Satellite (GOSAT) shortwave infrared measurements: performance comparison of proxy and physics retrieval algorithms, J. Geophys. Res.-Atmos., 117, D10307, doi:10.1029/2012JD017549, 2012. 11498, 11499, 11500, 11511, 11514

Schneising, O., Bergamaschi, P., Bovensmann, H., Buchwitz, M., Burrows, J. P., Deutscher, N. M., Griffith, D. W. T., Heymann, J., Macatangay, R., Messerschmidt, J., Notholt, J., Rettinger, M., Reuter, M., Sussmann, R., Velazco, V. A., Warneke, T., Wennberg, P. O., and Wunch, D.: Atmospheric greenhouse gases retrieved from SCIAMACHY: comparison to ground-based FTS measurements and model results, Atmos. Chem. Phys., 12, 1527–1540, doi:10.5194/acp-12-1527-2012, 2012. 11497

Simpson, I., Rowland, F. S., Meinardi, S., and Blake, D. R.: Influence of biomass burning during recent fluctuations in the slow growth of global tropospheric methane, Geophys. Res. Lett., 33, L22808, doi:10.1029/2006GL027330, 2006. 11496

Stocker, T., Qin, D., Plattner, G. K., Tignor, M., Allen, S. K., Boschung, J., Nauels, A., Xia, Y., Bex, V., and Midgley, P. M. (Eds.): Summary for Policymakers, Climate Change 2013: The Physical Science Basis, Contribution of Working Group I to the Fifth Assessment Report of the Intergovernmental Panel on Climate Change, Cambridge University Press, Cambridge, United Kingdom and New York, NY, USA, 2013. 11496

Tarantola, A.: Inverse Problem Theory and Methods for Model Parameter Estimation, Society for Industrial and Applied Mathematics, Philadelphia, PA, USA, 2004. 11496

Vermeulen, A. T., Schmidt, M., Manning, A., Moors, E., Moncrieff, J., Haszpra, L., Stefani, P., and Lindroth, A.: CHIOTTO: Final Project Report, Tech. Rep. ECN-E-07-052, ECN Petten, Petten, the Netherlands, 2007. 11496

WMO: WMO Greenhouse Gas Bulletin – the State of Greenhouse Gases in the Atmosphere Based on Global Observations through 2012, Geneva, Switzerland, 2013. 11496

Wofsy, S. C.: HIAPER Pole-to-Pole Observations (HIPPO): fine-grained, global-scale measurements of climatically important atmospheric gases and aerosols, Philos. T. R. Soc. A, 369, 2073–2086, doi:10.1098/rsta.2010.0313, 2011. 11503

ACPD
14, 11493–11539, 2014

Wunch, D., Toon, G. C., Wennberg, P. O., Wofsy, S. C., Stephens, B. B., Fischer, M. L., Uchino, O., Abshire, J. B., Bernath, P., Biraud, S. C., Blavier, J.-F. L., Boone, C., Bowman, K. P., Browell, E. V., Campos, T., Connor, B. J., Daube, B. C., Deutscher, N. M., Diao, M., Elkins, J. W., Gerbig, C., Gottlieb, E., Griffith, D. W. T., Hurst, D. F., Jiménez, R., Keppel-Aleks, G., Kort, E. A., Macatangay, R., Machida, T., Matsueda, H., Moore, F., Morino, I., Park, S., Robinson, J., Roehl, C. M., Sawa, Y., Sherlock, V., Sweeney, C., Tanaka, T., and Zondlo, M. A.: Calibration of the Total Carbon Column Observing Network using aircraft profile data, Atmos. Meas. Tech., 3, 1351–1362, doi:10.5194/amt-3-1351-2010, 2010. 11499, 11501, 11504, 11512, 11513

Yoshida, Y., Ota, Y., Eguchi, N., Kikuchi, N., Nobuta, K., Tran, H., Morino, I., and Yokota, T.: Retrieval algorithm for CO_2 and CH_4 column abundances from short-wavelength infrared spectral observations by the Greenhouse gases observing satellite, Atmos. Meas. Tech., 4, 717–734, doi:10.5194/amt-4-717-2011, 2011. 11497

ACPD
14, 11493–11539, 2014

Table 1. Satellite data used in the inversions.

Satellite/Instrument	Algorithm	Proxy CO_2 model	Data provider	Temporal data coverage
ENVISAT/SCIAMACHY	IMAP v5.5	CarbonTracker	SRON	Jan 2009–Mar 2012
GOSAT/TANSO-FTS	OCPR v4.0	LMDZ	Univ. of Leicester	Jun 2009–Dec 2011
GOSAT/TANSO-FTS	RemoTeC Proxy v1.9/v2.0	CarbonTracker	SRON/KIT	v1.9: Jan 2009–Oct 2011 v2.0: Oct 2011–Jun 2012
GOSAT/TANSO-FTS	RemoTeC FP v2.1	–	SRON/KIT	Jun 2009–Jun 2012

ACPD
14, 11493–11539, 2014

Table 2. Inversions.

Inversion	Assimilated observations
S1-NOAA	NOAA/ESRL surface measurements only
S1-GOSAT-SRON-PX	NOAA/ESRL surface measurements and GOSAT SRON RemoTeC v19/v20 XCH_4 retrievals
S1-GOSAT-SRON-FP	NOAA/ESRL surface measurements and GOSAT SRON FP v2.1 XCH_4 retrievals
S1-GOSAT-UL-PX	NOAA/ESRL surface measurements and GOSAT OCPR v4.0 XCH_4 retrievals
S1-SCIA	NOAA/ESRL surface measurements and SCIAMACHY IMAP v5.5 XCH_4 retrievals
S2-GOSAT-SRON-FP	as S1-GOSAT-SRON-FP, but constant bias correction instead of 2nd order polynomial
S3-GOSAT-SRON-FP	as S1-GOSAT-SRON-FP, but smooth bias correction
S2-GOSAT-UL-PX	as S1-GOSAT-UL-PX, but constant bias correction instead of 2nd order polynomial
S3-GOSAT-UL-PX	as S1-GOSAT-UL-PX, but smooth bias correction

ACPD
14, 11493–11539, 2014

Table 3. Statistics for inversions S1-NOAA through S1-SCIA: NOAA surface measurements (left) and satellite data (right). See Fig. 3 for the frequency distributions of fit residuals.

Inversion	NOAA ground stations			Satellite		
	n	Bias [ppb]	RMS [ppb]	*n*	Bias [ppb]	RMS [ppb]
S1-NOAA	3418	0.2	11.5	–	–	–
S1-GOSAT-SRON-PX	3418	0.3	12.4	106 872	−0.3	9.2
S1-GOSAT-SRON-FP	3418	0.4	12.1	31 201	−0.3	10.4
S1-GOSAT-UL-PX	3418	0.4	11.8	129 916	−0.1	8.9
S1-SCIA	3418	0.3	12.0	432 008	−0.9	32.3

ACPD
14, 11493–11539, 2014

Table 4. 2 year average CH_4 emissions for the TRANSCOM land regions and optimized source categories (in $Tg\,CH_4\,yr^{-1}$). The prior emission inventories are as used by Bergamaschi et al. (2013a). The global emission totals include the contributions of ice and ocean regions.

Region	A priori	S1-NOAA	S1-GOSAT-SRON-PX	S*-GOSAT-SRON-FP			S*-GOSAT-UL-PX			S1-SCIA
				S1	S2	S3	S1	S2	S3	
BNA	13.0	11.5	11.0	12.2	13.3	12.2	10.3	11.4	10.2	10.3
TNA	38.5	47.6	41.3	44.8	41.3	43.1	52.1	47.3	51.5	45.6
TrSA	63.7	74.9	70.0	79.4	79.6	80.7	70.7	72.4	71.6	71.8
TSA	37.5	40.9	41.4	41.7	41.5	40.5	41.3	42.3	40.7	40.2
NAf	36.7	43.0	35.5	48.0	52.7	48.1	38.3	41.7	40.2	50.6
SAf	28.5	36.4	43.6	36.4	37.7	36.2	38.4	40.0	35.7	42.0
BEr	18.1	18.1	18.7	16.8	16.7	17.0	17.0	17.4	16.7	15.4
TEr	131.4	110.1	112.7	110.4	104.7	108.9	104.0	98.1	103.0	109.6
TrAs	69.6	75.9	73.2	67.7	73.4	68.6	77.2	81.4	77.4	76.8
Aus	5.8	4.8	7.7	4.7	3.5	4.4	6.9	6.2	7.8	4.3
Eur	46.4	29.5	39.5	33.8	29.0	35.7	36.8	32.9	38.0	28.9
Global totals	535.5	538.1	536.9	537.7	537.9	537.2	538.2	538.2	538.4	540.5

ACPD
14, 11493–11539, 2014

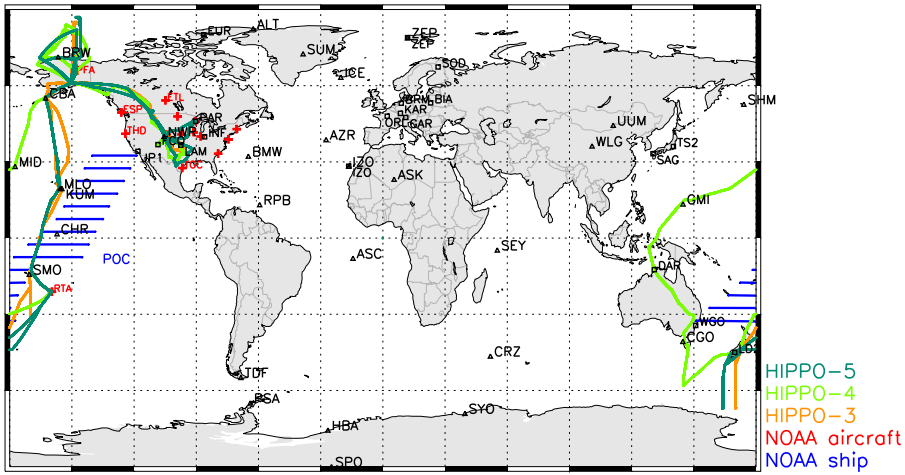

Fig. 1. Observation data map indicating the locations of NOAA surface stations used in the inversions (see also Table T1 in the Supplement). The white squares indicate the TCCON station locations. Some of the NOAA and TCCON stations are co-located. The regions covered by NOAA ship cruises (labeled as POC) are displayed through the horizontal blue lines, which indicate the longitudinal range within each 5° latitude band. In addition, we show the NOAA aircraft profile locations (red crosses), and the HIPPO 3–5 transects used for validation.

ACPD
14, 11493–11539, 2014

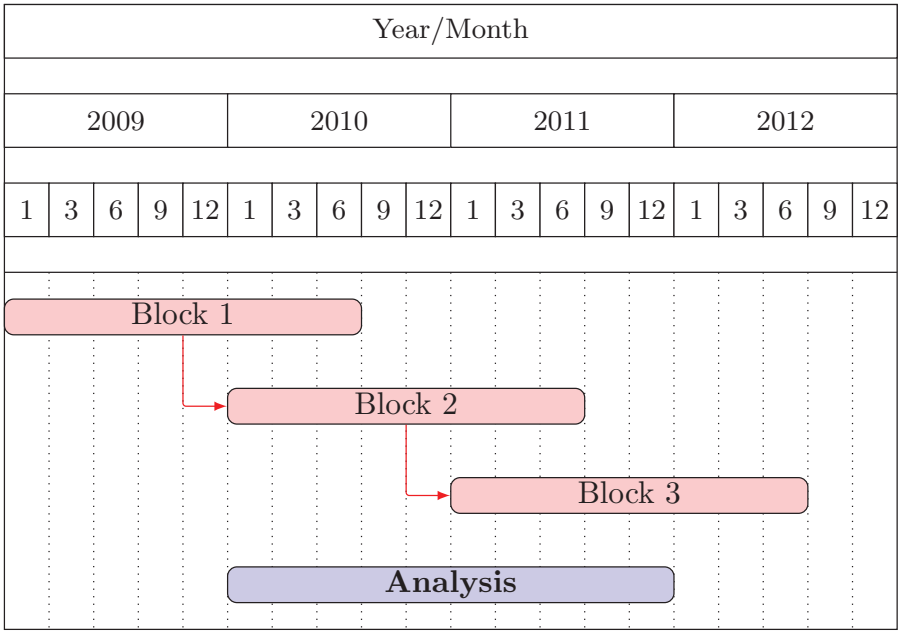

Fig. 2. The inversion settings, as described in Sect. 3.2. Inversion blocks 2 and 3 start (on 1 January 2010, and 1 January 2011, respectively) from the optimized 3-D CH_4 fields calculated by the previous block.

ACPD
14, 11493–11539, 2014

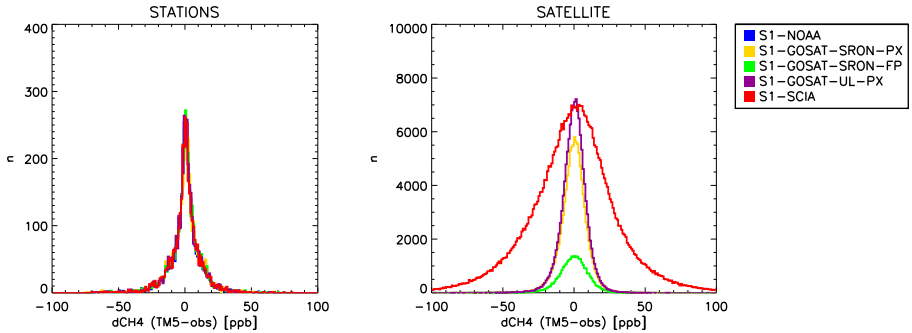

Fig. 3. Frequency distributions of model–observation residuals (dCH_4) for satellite and station data (2010–2011). Both station and satellite data are distributed across 1 ppb bins. The total number of measurements falling inside a bin is denoted by *n*. The bias, standard deviation and RMS of each inversion are shown in Table 3.

ACPD
14, 11493–11539, 2014

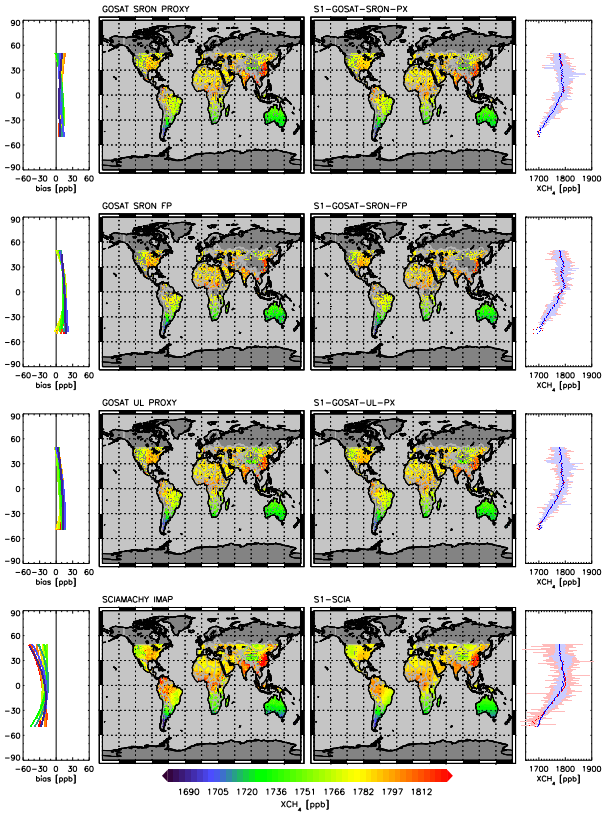

Fig. 4. Column-averaged CH_4 mixing ratios (XCH_4): bias-corrected satellite retrievals vs. TM5-4DVAR. The leftmost plots show the monthly average bias corrections (in ppb) applied to the satellite data for January 2010–December 2011. The panels on the right display the 2 year latitudinal average XCH_4 values (red: satellite, blue: TM5-4DVAR) and the corresponding minimum and maximum values across the longitude.

ACPD
14, 11493–11539, 2014

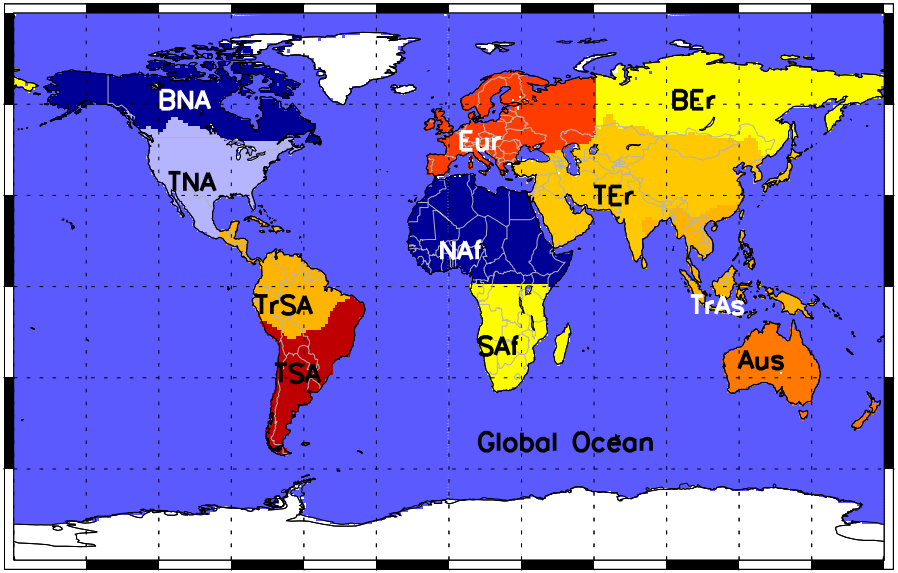

Fig. 5. The TRANSCOM emission regions used in this study (at 1° × 1° resolution). The land regions are labeled as follows: Boreal North America (BNA), Temperate North America (TNA), Tropical South America (TrSA), Temperate South America (TSA), Europe (Eur), North Africa (NAf), South Africa (SAf), Boreal Eurasia (BEr), Temperate Eurasia (TEr), Tropical Asia (TrAs), and Australasia (Aus). White areas (ice) are not assigned to any region.

ACPD
14, 11493–11539, 2014

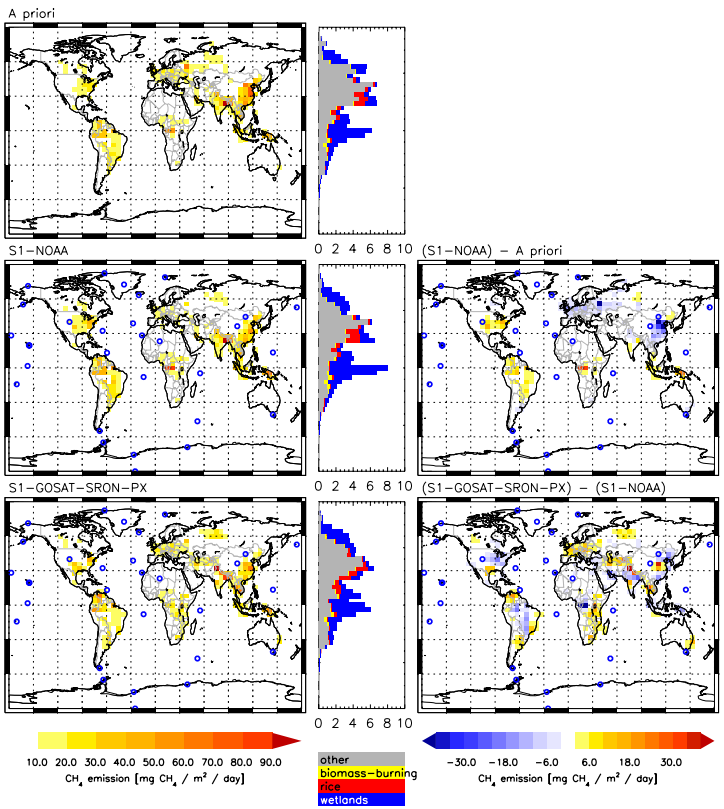

Fig. 6. Left: a posteriori 2 year average emissions for S1-NOAA and S1-GOSAT-SRON-PX. White areas indicate very small changes over the prior (less than 10 mg CH_4 m^{-2} day^{-1}). The a priori emissions are shown in the topmost plot. The differences among scenarios are shown in the rightmost panels. The middle plots show the partitioning among the four source categories that have been optimized in this study (2 year latitudinal averages).

ACPD
14, 11493–11539, 2014

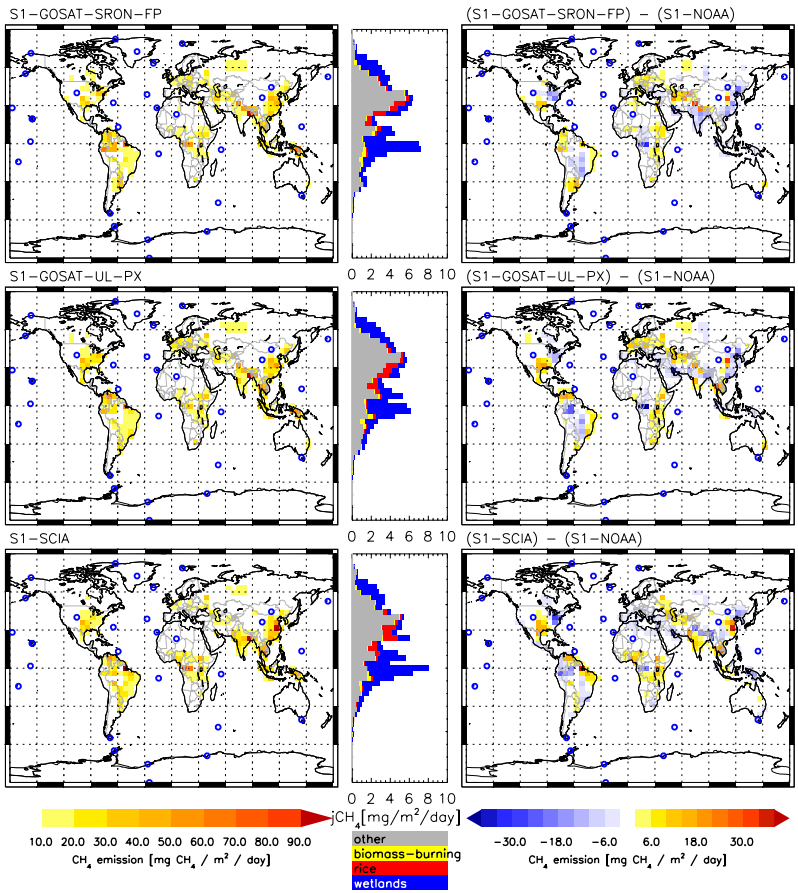

Fig. 6. Continued – scenarios S1-GOSAT-SRON-FP – S1-SCIA.

ACPD
14, 11493–11539, 2014

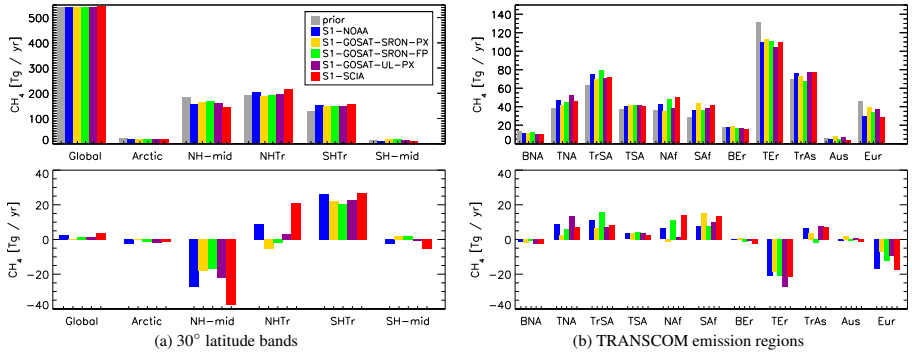

Fig. 7. Average yearly CH_4 emissions for the pre-defined regions. Top panels show total surface fluxes (in $Tg\,CH_4\,yr^{-1}$), while increments from the prior are given in the bottom panels. Yearly totals are shown in **(a)**, along with surface fluxes attributed to each 30° latitude band. The Antarctic region (not shown here) is estimated to be responsible for less than $0.1\,Tg\,yr^{-1}$ of CH_4. See Fig. 5 for the definition of the modified TRANSCOM regions shown in **(b)**.

ACPD
14, 11493–11539, 2014

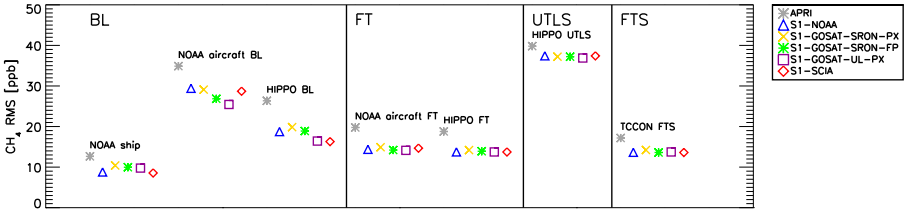

Fig. 8. Validation against independent measurement data sets for all inversions. A priori (APRI) values are taken from scenario S1-NOAA, starting from optimized 3-D CH_4 fields at the beginning of each year. The plot shows the RMS (in ppb) of differences between modeled methane mixing ratios, and observation data in the boundary layer ("BL"), free troposphere ("FT"), and upper troposphere/lower stratosphere ("UT/LS"). Observation data sources: NOAA shipboard samples, vertical profiles from NOAA aircraft sampling, and the HIPPO campaigns 3–5. Validation results for the Fourier Transform Spectrometer CH_4 total column data from TCCON are shown in a separate panel ("FTS").

ACPD
14, 11493–11539, 2014

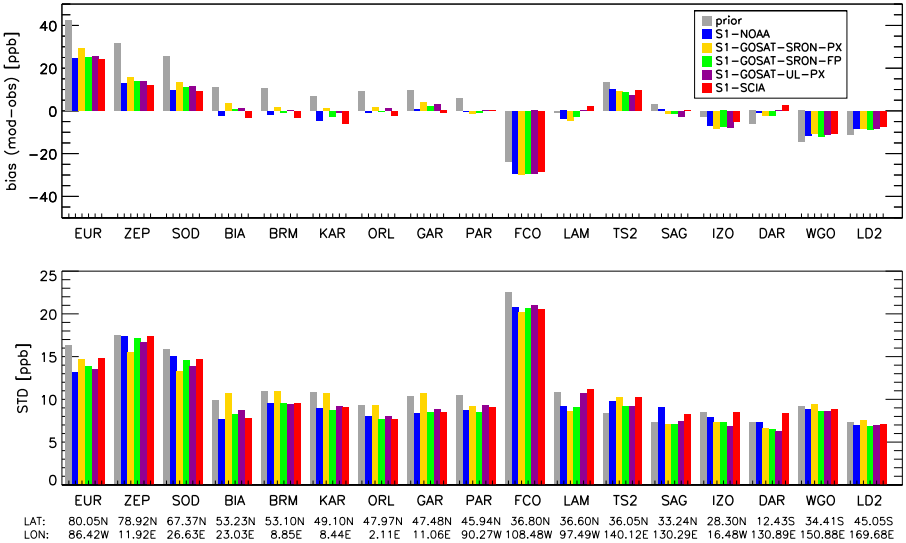

Fig. 9. Model validation against TCCON data across all measurement stations with significant data coverage during our inversion period. Prior values are given by the grey bars. Upper panel: bias (in ppb). Lower panel: standard deviation.

ACPD
14, 11493–11539, 2014

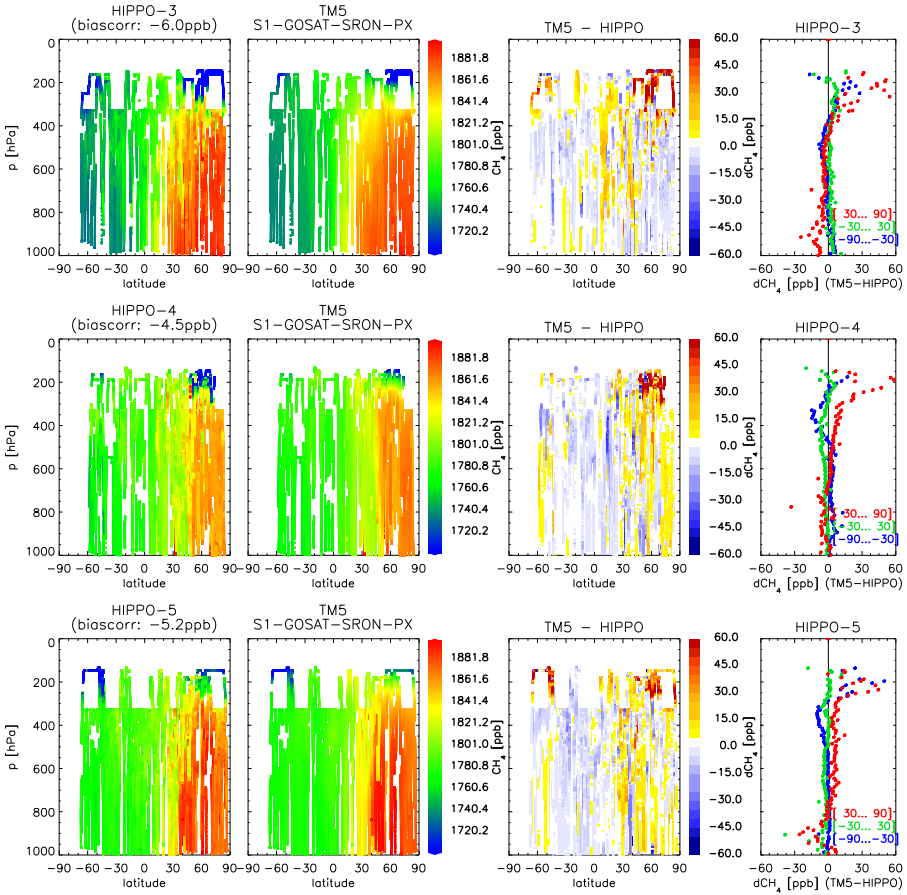

Fig. 10. Scenario S1-GOSAT-SRON-PX: validation against HIPPO campaigns 3–5 (southbound and northbound flights). Rightmost panels show the average bias as a function of latitude: extra-tropical Northern Hemisphere (NH) in red, extra-tropical SH in blue, and the tropics in green. HIPPO validation results for the other inversions are shown in the Supplement.

ACPD
14, 11493–11539, 2014